Molecular Dynamics Simulations and Instantaneous Normal-Mode Analysis of the Vibrational Relaxation of the C−H Stretching Modes of *N*-methylacetamide-*d* in Liquid Deuterated Water

Adolfo Bastida,*,† Miguel A. Soler,† José Zúñiga,† Alberto Requena,† Adrián Kalstein,‡ and Sebastian Fernández-Alberti‡

Departamento de Química Física, Universidad de Murcia, 30100 Murcia, Spain, and Universidad Nacional de Quilmes, Roque Saenz Peña 352, B1876BXD Bernal, Argentina

Nonequilibrium molecular dynamics (MD) simulations and instantaneous normal mode (INMs) analyses are used to study the vibrational relaxation of the C−H stretching modes ($\nu_s(CH_3)$) of deuterated *N*-methylacetamide (NMAD) in aqueous (D_2O) solution. The INMs are identified unequivocally in terms of the equilibrium normal modes (ENMs), or groups of them, using a restricted version of the recently proposed Min-Cost assignment method. After excitation of the parent $\nu_s(CH_3)$ modes with one vibrational quantum, the vibrational energy is shown to dissipate through both intramolecular vibrational redistribution (IVR) and intermolecular vibrational energy transfer (VET). The decay of the vibrational energy of the $\nu_s(CH_3)$ modes is well fitted to a triple exponential function, with each characterizing a well-defined stage of the entire relaxation process. The first, and major, relaxation stage corresponds to a coherent ultrashort ($\tau_{rel} = 0.07$ ps) energy transfer from the parent $\nu_s(CH_3)$ modes to the methyl bending modes $\delta(CH_3)$, so that the initially excited state rapidly evolves into a mixed stretch−bend state. In the second stage, characterized by a time of 0.92 ps, the vibrational energy flows through IVR to a number of mid-range-energy vibrations of the solute. In the third stage, the vibrational energy accumulated in the excited modes dissipates into the bath through an indirect VET process mediated by lower-energy modes, on a time scale of 10.6 ps. All the specific relaxation channels participating in the whole relaxation process are properly identified. The results from the simulations are finally compared with the recent experimental measurements of the $\nu_s(CH_3)$ vibrational energy relaxation in NMAD/D_2O(l) reported by Dlott et al. (*J. Phys. Chem. A* **2009**, *113*, 75.) using ultrafast infrared-Raman spectroscopy.

1. Introduction

Vibrational energy relaxation (VER) plays a fundamental role in a multiple variety of relevant biological processes such as protein−ligand interactions,[1,2] allosteric regulations,[3,4] agonist binding,[5] and ATP-binding.[6] The excess of vibrational energy, initially localized in bond stretching or bending vibrations, follows processes of intramolecular vibrational energy redistribution (IVR) and/or intermolecular vibrational energy transfer (VET).[7–10] Experiments and simulations on energy flow through a polypeptide competing with energy flow to the solvent have also been reported recently.[10–21] Specific pathways of IVR and VET act as links in the structure−function relationship of proteins. Furthermore, sets of interacting residues from evolutionary conserved pathways through the protein allow efficient energy conduction within proteins.[22]

A rich variety of vibrational spectroscopies can be used in understanding the dynamic properties of molecules of biological interest. Among them, ultrafast time-resolved infrared and Raman spectroscopic techniques[23–34] have been revealed as being suitable for investigating the vibrational energy flows throughout the molecule. Nowadays, the capabilities of such techniques to determine the structures and conformational dynamics of proteins is well established.[29,35] A resolution in time of several

hundred femtoseconds provides information on IVR and VET channels after laser excitation of specific vibrational modes.[23,27,36]

In this context, special attention has been paid to the vibrational energy relaxation of the amide bond. The importance of the amide group lies in its role in determining the topology of the hydrogen-bonded network that defines the secondary structure of proteins. The amide I band, which mainly involves the C=O stretching of the amide bond, is widely used as a marker for secondary structure, dynamics, and hydrogen-bonding pattern.[26,37–40] It has also been largely employed in unraveling the molecular origin of VER in molecules with peptide bonds like *N*-methylacetamide (NMA), small peptides, and large proteins.[26,28,41,42] Despite the sensitivity of the frequency and shape of the amide I band to hydrogen-bonding and conformation, time-domain measurements show that this mode has a lifetime close to 1 ps for all systems considered.[26] This finding validates the use of NMA as a simple model for the amide bond in peptides and proteins, something that is corroborated by the vast number of experimental[26,28,32,38,41,43–47] and theoretical[44,48–57] studies reporting on this system. A common agreement has been achieved that the vibrational relaxation of the amide I mode takes place mainly through specific IVR channels in which mid-range vibrational modes play a significant role.

From the theoretical point of view, the different approaches applied to the NMA system do not, however, provide a uniform level of agreement with the experimental measurements. Most of these studies have focused on the VER of the amide I mode.

* To whom correspondence should be addressed E-mail: bastida@um.es.
† Universidad de Murcia.
‡ Universidad Nacional de Quilmes.

On the one hand, perturbative Fermi's Golden Rule approaches with classical force−force correlation function[1,29,58–61] give decay times of about 2 orders of magnitude larger than experiment,[49] which improve when more realistic treatments of the inhomogeneous environment are used.[53,55,62] Although these methods are limited to short time regime dynamics, they have allowed the dominant relaxation pathways to be identified as essentially IVR processes. On the other hand, applications of nonequilibrium molecular dynamics have revealed that the amide I energy relaxation has a biexponential nature.[49,57]

A large number of MD simulations in biomolecules use the equilibrium normal modes (ENMs) analysis to elucidate vibrational motions.[63–66] Anharmonic decay rates of the normal modes of helical and coil segments of myoglobin, calculated by perturbation theory, have been analyzed and discussed in detail by Leitner et al.[11,42,67] The energy transfer rates obtained in this way incorporate the quantum occupation number of each normal mode at the desired temperature. Furthermore, thermal transport coefficients, coefficients of thermal conductivity, and thermal diffusivity have been calculated for proteins.[42] All this work shows that anharmonicity enhances heat flow by transferring energy among localized normal modes; that is, that energy transfer occurs predominantly by hopping of localized vibrations. This behavior has also been shown to mimic that of an anharmonic one-dimensional glass. The flow of vibrational energy can be addressed then by following the time evolution of the kinetic energy of each ENM.[68,69] Since the ENMs arise from diagonalization of the Hessian matrix at the local minimum of the potential, the application of this methodology to biomolecules, which usually have a large number of minima mutually accessible at room temperature, is somehow questionable. In addition, the vibrational anharmonicities and couplings eventually make it quite difficult to quantify the energy stored in each individual ENM.[49] An alternative way to undertake this problem is to use the instantaneous normal modes (INMs),[70–72] which are obtained by diagonalizing the Hessian matrix at each instantaneous configuration of the molecule. While the ENMs provide a natural way of interpreting of the experimental vibrational spectra, the INMs provide an instantaneous decoupled second-order description of the vibrational motions of the molecule at the corresponding time-dependent configuration. The INMs therefore evolve with time, which complicates their identification. In previous works,[57,73] we have proposed a method to assign unequivocally the INMs in terms of the ENMs on the basis of the use of the so-called Min-Cost algorithm and applied it successfully to study the vibrational relaxation of the amide I mode of deuterated NMA (NMAD) in liquid deuterated water by nonequilibrium MD simulations.

Very recently, VER in polyatomic molecules has been studied in unprecedented detail by Dlott et al.[47] using ultrafast time-resolved infrared-Raman spectroscopy. In this work, the CH-stretch transition of glycine, NMA, and benzoate anion is pumped by a short-duration IR pulse, and a time series of anti-Stokes Raman spectra is acquired that measures the time-dependent populations of several vibrational modes excited after CH-stretch relaxation. In addition, intermolecular VET to the solvent molecules is followed in time by observing the Raman spectrum of the aqueous medium.[74,75] The results extracted from these experiments are interpreted by using a common three-stage model for VER.[47,76] While the VER process in glycine is mainly statistical, specific relaxation channels are identified in NMA and benzoate anion. Among these three solutes, NMA is the molecule in which the largest number of vibrations are tested, making this molecule the most representative to study VER in

depth by nonequilibrium MD simulations assisted by INMs analysis. This is therefore the objective of this work.

We have accordingly carried out nonequilibrium MD simulations of the vibrational relaxation of the C−H stretches of NMAD in aqueous D_2O solution and identified the corresponding relaxation channels by monitoring the energy stored in the individual vibrational modes using the INMs description. This methodology allows us to directly compare the results from the simulations with the corresponding experimental transient Raman data. MD simulations using constraints applied to specific vibrations of the system are also performed to elucidate the mechanism of VER. The specific pathways of IVR and VET are thus identified and discussed, emphasizing the comparison with the recent ultrafast infrared-Raman spectroscopic measurements.[47] The paper is organized as follows. In section 2 we describe the propagation MD scheme used and the INM analysis carried out and give the computational details. In section 3 we present and discuss the results extracted from the simulations and compare them with the experiments. Conclusions are given in section 4.

2. Methodology

2.1. Energy Partition and Propagation Coordinates. Since the methodology on the propagation of the system has been described in detail elsewhere,[57] only a brief outline is given here. The total energy of the system is expressed as the sum

$$E_{tot} = E_{NMAD} + E_{D_2O_{(l)}} + V_{NMAD/D_2O_{(l)}} \tag{1}$$

where E_{NMAD} and $E_{D_2O_{(l)}}$ are the energies depending, respectively, on the solute and the solvent coordinates and $V_{NMAD/D_2O_{(l)}}$ is the intermolecular potential energy between the NMAD molecule and the solvent.

The NMAD motions are described using the set of coordinates $\{\mathbf{R}_{CM}, \mathbf{q}, \mathbf{Q}^e\}$, where $\mathbf{R}_{CM}$ is the center of mass vector, $\mathbf{q} = (q_1, q_2, q_3, q_4)$ are the quaternions that specify the rotation of the molecule, and $\mathbf{Q}^e = (Q_1^e, ..., Q_N^e)$ are the ENMs that describe the vibrational motions. If the rotational−vibrational couplings are neglected,[56] the NMAD energy is in turn partitioned as follows

$$E_{NMAD} = E_{NMAD}^{trans} + E_{NMAD}^{rot} + E_{NMAD}^{vib} \tag{2}$$

where E_{NMAD}^{trans}, E_{NMAD}^{rot}, and E_{NMAD}^{vib} are respectively the corresponding translational, rotational, and vibrational contributions. The choice of the ENMs as vibrational coordinates allows us to write the term E_{NMAD}^{vib} as

$$E_{NMAD}^{vib} = \frac{1}{2} \sum_{i=1}^{N} (\dot{Q}_i^e)^2 + V_{NMAD}(\mathbf{Q}^e) \tag{3}$$

where $N = 30$ is the number of vibrational degrees of freedom and $V_{NMAD}(\mathbf{Q}^e)$ is the intramolecular potential energy function. Direct use of the ENMs also enables us to carry out MD simulations restricted to some specific normal modes straightforwardly to check the viability of the different relaxation pathways of the system.

2.2. INM Analysis. The flow of vibrational energy within the solute molecule can be analyzed, in principle, by tracking the time evolution of the energy stored in each ENM,[68,69] under the assumption that the intramolecular potential energy

function is expressed accurately as the sum of the independent ENM harmonic oscillators. This is certainly the case for molecular configurations that are close to the equilibrium geometry. Due to interactions with the solvent and to its proper thermal motions,[77,78] biomolecules in solution at room temperature explore quite easily regions of the phase space which are far away from the equilibrium one, and this heavily complicates the use of the ENMs description to analyze the dynamics of the molecule over time.[49] A useful alternative in this respect is to resort to the INMs, which are defined as the vibrational coordinates that diagonalize the Hessian matrix at the successive configurations of the molecule,[70–72] thus providing instantaneous decoupled second-order descriptions of the vibrational motions of the solute molecule as it evolves with time.

The use of the INMs to analyze the vibrational dynamics of a given system requires an efficient method to assign them at each instantaneous configuration and to connect the successive time-dependent INM sets according to their assignments to identify each individual INM along the dynamics of the system. To achieve this, it is convenient to express the INMs in terms of the ENMs, and this can be done by expanding the sum of the V_{NMAD} and $V_{NMAD/D_2O(l)}$ potentials in a power series of the ENMs about the configuration of the molecule at a given time t_0, and by then diagonalizing the corresponding Hessian matrix. Thus, we find the following relationship between the INMs and the ENMs,[57]

$$Q_i^{INM} = \sum_{j=1}^{N} l_{ji}(Q_j^e - Q_j^e(t_0)) \qquad (4)$$

in which l_{ji} are the elements of the eigenvector matrix **L**. It is shown then[57] that the total vibrational energy of the solute, E_{NMAD}^{vib}, can be written in terms of the INMs up to second order, as follows

$$E_{NMAD}^{vib} = V_0 + \sum_{i=1}^{N} E_i^{INM} \qquad (5)$$

where E_i^{INM} is the vibrational energy of the ith INM given by

$$E_i^{INM} = \frac{1}{2}(\dot{Q}_i^{INM})^2 + \frac{1}{2}\lambda_i(Q_i^{INM} + a_i)^2 \qquad (6)$$

and a_i and V_0 are respectively coordinate and potential shifts from the equilibrium configuration.[57] The vibrational frequencies of the INMs are given by $\nu_i = (\lambda_i)^{1/2}/2\pi$, where λ_i are the eigenvalues of the Hessian matrix.

Equations 5 and 6 demonstrate that the vibrational energy of the solute can be quantified as a sum of the individual INM contributions, thereby allowing us to evaluate the averaged values and populations of the individual vibrational modes as a function of time and, thus, compare them with the observed values extracted from time-resolved infrared-Raman experiments. As commented above, to accomplish this, it is necessary to assign properly the INMs at each instantaneous configuration so as to use the corresponding assignment labels to track the identities of the individual INMs with time.

In previous works,[57,73] we have developed an efficient method to assign the INMs based on the use of the ENMs as templates. The method proceeds by selecting those elements of the eigenvector matrix **L**, one for each row and each pertaining to

a different column, which maximizes the sum of their squared values, and thus provides a unique relationship between the two sets of normal modes. We employ the so-called Min-Cost or Min-Sum algorithm,[79] duly adapted to our problem (see refs 57 and 73), to get the set of l_{ij}^2 elements that maximizes the overlaps between the INMs and the ENMs at each instantaneous configuration. We note that the INMs analysis is fully independent of the MD propagation. The INMs are then calculated and assigned to individual ENMs only when required along the nonequilibrium MD trajectories. Typically, the INMs analysis is performed at time intervals longer than the time propagation step, to reduce the number of numerical diagonalizations of the ENMs Hessian matrices, since this last task can be computationally very demanding, especially for big solute molecules. Direct application of the Min-Cost assignment method may lead occasionally to unphysical assignments (see below) of the INMs when two or more present significant contributions of ENMs with very different frequencies, thereby making it quite difficult to track the identities of the corresponding INMs. To fix this shortcoming, we have included restrictions in the method[73] consisting basically of limiting its application to frequency ranges of width $\Delta\omega$ centered at the ENM frequencies ω_i^e. Thus, only those INMs whose frequencies lie in the window ($\omega_i^e - \Delta\omega/2$, $\omega_i^e + \Delta\omega/2$) are candidates for assignment to the ith ENM. This restriction is accomplished by assigning arbitrary low values to the corresponding l_{ij}^2 elements.

When applying the direct Min-Cost assignment method to the INMs of the NMAD molecule in water D_2O solution, we find that the low-frequency 1st and 2nd, and the high-frequency 25th and 26th INMs share noticeable contributions of the corresponding 1st, 2nd, 25th, and 26th ENMs.[73] Erroneous assignments of the 25th and 26th INMs to the 1st and 2nd ENMs are then expected to occur, and they certainly do, as these modes evolve with time, making their identifications very problematic. Since the 25th and 26th INMs correspond exactly to the, initially excited, C−H stretching modes, it then becomes mandatory to use the restricted Min-Cost assignment method to monitor the relaxation dynamics of these modes. For the NMAD/D_2O(l) system, a $\Delta\omega = 400$ cm^{-1} frequency window was found to be optimal to prevent undesirable assignments without excessively sacrificing the efficiency of the Min-Cost method.[73]

In Table 1 we give the time averaged frequencies of the INMs of NMAD assigned using the restricted Min-Cost method, along with the corresponding time averaged highest l_{ij}^2 contributions of the ENMs to the INMs. For the first three INMs we have found in our simulations trajectories with negative force constants λ_i, which give imaginary frequencies. When averaged, only the vibrational frequency of the first INM remains imaginary and its value is taken to be negative, as is usually done.[70–72] The mean value of the time-averaged overlaps l_{ij}^2 included in Table 1 is 0.47. We note that this value obtained using the restricted Min-Cost method is noticeably higher[57,73] than that provided by the simple frequency ordering identification method of the INMs, which is 0.32 and only slightly smaller than the maximun average overlap 0.55 obtained using the direct Min-Cost algorithm.[57]

Despite the improvements achieved in the assignments of the INMs by using the Min-Cost method, there are INMs that cannot be unambiguously assigned to a single ENM, as is clearly observed in Table 1, due to recurrent crossed assignments during the simulations. These mixed INMs are gathered in groups according to their nearly degenerated time-averaged vibrational frequencies. In order of ascending frequency, we have first the group a_1 of modes composed of the 11th to 15th INMs, which

TABLE 1: Time Averaged Vibrational Frequencies (cm^{-1}) of the INMs of the NMAD Molecule in D$_2$O(l) and Averaged Values of the Highest Contributions of the ENMs to the INMs Obtained Using the Restricted Min-Cost Assignment Method with a Frequency Window of Width $\Delta\omega = 400$ cm^{-1}

	INM	Frequency	Max. overlap	Label[a]
	1[b]	-94.4 ± 286.9	0.24	τ(CH$_3$)
	2[b]	19.7 ± 308.1	0.25	τ(CH$_3$)
	3[b]	196.2 ± 126.8	0.51	τ(CN)
	4	311.9 ± 31.4	0.76	δ(CNC)
	5	453.9 ± 14.7	0.85	δ(CCN)
	6	457.4 ± 178.2	0.65	amide V
	7	592.6 ± 10.6	0.84	amide IV
	8	646.3 ± 42.3	0.57	amide VI
	9	778.6 ± 21.8	0.76	ν(CC)
	10	831.2 ± 33.1	0.67	amide III
group a_1	11	1040.2 ± 71.0	0.37	$r \parallel$(CH$_3$)C
	12	1050.2 ± 78.3	0.27	$r \perp$(CH$_3$)N
	13	1050.8 ± 66.3	0.30	$r \parallel$(CH$_3$)N
	14	1033.4 ± 78.7	0.29	$r \perp$(CH$_3$)C
	15	1093.2 ± 43.4	0.37	ν(CN)
group a_2	16	1401.9 ± 48.4	0.30	δ_s(CH$_3$)C
	17	1397.0 ± 47.3	0.26	δ_a(CH$_3$)N
	18	1401.1 ± 51.8	0.27	δ_s(CH$_3$)C
	19	1400.5 ± 49.4	0.25	δ_s(CH$_3$)N
	20	1404.9 ± 52.5	0.26	δ_a(CH$_3$)C
	21	1537.7 ± 44.4	0.51	δ_s(CH$_3$)N
	22	1614.9 ± 22.4	0.71	amide II
	23	1691.8 ± 8.0	0.91	amide I
	24	2432.5 ± 7.1	0.97	amide A
group b_1	25	2845.2 ± 40.3	0.30	ν_s(CH$_3$)C
	26	2842.1 ± 42.9	0.30	ν_s(CH$_3$)N
group b_2	27	2982.2 ± 20.1	0.31	ν_a(CH$_3$)N
	28	2984.2 ± 15.8	0.31	ν_s(CH$_3$)N
	29	2985.7 ± 19.4	0.31	ν_a(CH$_3$)C
	30	2987.2 ± 18.5	0.31	ν_s(CH$_3$)C

[a] From ref 102. τ = torsion, δ = bending, ν = stretching, r = rocking, a = asymmetric, and s = symmetric. [b] Imaginary frequencies are given as negative frequencies.
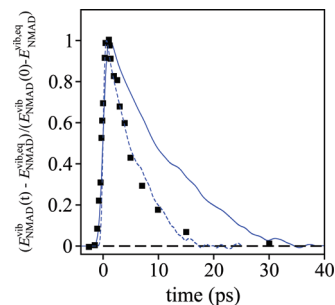

Figure 1. Normalized vibrational energy of the NMAD molecule, relative to its equilibrium value, calculated using eq 3 (blue line) and measured by Dlott et al.[47] (closed squares). The blue dashed line corresponds to the results from the simulations with the time axis scaled by a factor of 0.5. All the simulations results are convoluted using a Gaussian function with a fwhm of 1.4 ps.

are mainly formed by combinations of the rocking methyl ENMs and a backbone ENM mode. Then, we have group a_2, composed of the 16th to 20th INMs, with their highest contributions coming from the bending methyl ENMs. Next, comes group b_1, containing the 25th and 26th INMs, which are composed essentially of the C−H stretches (ν_s(CH$_3$)) excited in the simulations, and finally we have group b_2, formed by the 27th to 30th INMs, which are made up basically of the more energetic stretching methyl ENMs. We note that the present definitions of groups of INMs are fairly different and more precise than those presented in our previous work[57] where the direct Min-Cost algorithm was applied.

2.3. Computational Details. The nonequilibrium MD simulations of the vibrational relaxation of the C−H stretching modes of deuterated *N*-methylacetamide (H$_3$C−COND−CH$_3$) in aqueous (D$_2$O) solution have been performed by placing a NMAD molecule and a number of 251 D$_2$O molecules in a cubic box of 1.975 nm length, so as to reproduce the experimental density[80] ($\rho = 1.10436$ g/cm^3). We have used the AMBER force field[81] to model the solute NMAD, and the flexible TIP3P water model with doubled hydrogen masses included in the CHARMM[82] force field to represent the D$_2$O solvent. This water model has been chosen, in particular, because it provides a bending normal-mode frequency ω_b of 1264.7 cm^{-1}, which is quite close to the experimental value.[83] Subroutines of the TINKER modeling package[84] are also used in our code to evaluate the forces and the potential energy function. Periodic boundary conditions are

imposed to simulate the bulk system, and a cutoff of 10 Å is applied to nonbonded interactions.

The equations of motion were integrated by using the leapfrog algorithm with a time step of 0.5 fs for all coordinates, except for the quaternions, which were propagated using the mid-step implicit leapfrog rotational algorithm proposed by Svanberg.[85] The ENMs of the NMAD molecule that were employed to propagate the vibrational motions and to assign the INMs are those corresponding to the optimized geometry of the *trans-cc*-NMA conformer, as in our previous works.[57,73] The initial coordinates for the vibrational relaxation dynamics were taken from 16 previous molecular dynamics simulations of 1250 ps at 300 K, started using random velocities. An initial period of time of 750 ps was used to equilibrate the system, collecting data at 20 ps intervals in the last 500 ps. During the simulations the temperature was maintained at a mean value of 300 K by coupling to a thermal bath[86] with a time constant of 0.1 ps. Thus, 400 sets of initial positions and momenta were stored for subsequent nonequilibrium vibrational relaxation simulations. At $t = 0$, the energy corresponding to one vibrational quantum was suddenly deposited in the NMAD molecule by displacing one of the ν_s(CH$_3$) modes until its energy reached the proper value (see eq 6). Then the transformation matrix **L** (see section 2.2) was used to obtain the initial values of the ENMs.

The simulations of the relaxation process were performed in the *NVE* ensemble to avoid any influence of the velocity scaling on the results. Accordingly, two sets of 400 trajectories of 50 ps were propagated corresponding to the excitation of the 25th and 26th ν_s(CH$_3$) stretching modes, which form group b_1. Due to the strong mixing between these vibrational modes no significant differences were found in the results extracted from each set of trajectories. Accordingly, the results presented in this work are those obtained by averaging over all the trajectories, irrespective of the b_1 mode in which the excess of one quantum of vibrational energy was initially deposited.

3. Results and Discussion

3.1. Vibrational Relaxation of the NMAD Molecule. We have analyzed first the vibrational energy relaxation of the whole NMAD molecule in liquid D$_2$O after the excitation of the ν_s(CH$_3$) modes. In Figure 1 we plot the total vibrational energy of the molecule as a function of time, extracted from the simulations, and compare it with the vibrational energy relaxation measured by Dlott et al. using ultrafast time-resolved infrared-Raman spectroscopy.[47] A convolution was applied to the simulation results using a Gaussian function with a fwhm of 1.4 ps equal to the duration of the infrared laser pulse used
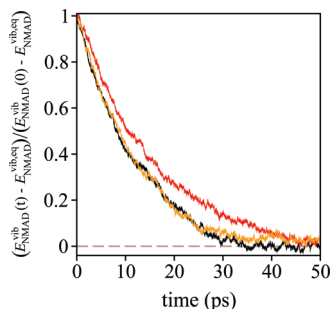
Figure 2. Normalized vibrational energy of the NMAD molecule, relative to its equilibrium value, obtained using the flexible (black), rigid (red), and semirigid with only the OD distances frozen (orange) models of the D_2O solvent.

Figure 3. Vibrational energy of the $\nu_s(CH_3)$ modes (group b_1) of NMAD, relative to its equilibrium value. We show in the inset the decay curve in the very first stage of the relaxation process.

in the experiments, to make a proper comparison with the experimental data. The decay of the total vibrational energy of the NMAD molecule extracted from the simulations follows a single-exponential function, with a relaxation time of 11.7 ps. This time is slightly higher than twice the experimental value measured by Dlott et al.[47] of 5.1 ps. As we will see below, the origin of this discrepancy lies in the lower rate of intermolecular VET to the solvent provided by the MD simulations.

In a recent study, Stock et al.[87] have carried out MD simulations of the cooling of hot NMA in water, which yield an overall cooling time of 5 ps, in good agreement with experiment. We should note here that there are some noticeable differences between that study and ours. In the Stock et al. work, H_2O is used as solvent, instead of D_2O, the N—H bond is frozen, and the methyl groups are described as united atoms, whereas we explicitly consider the motions of all atoms of the NMA molecule, and finally an initial temperature jump of NMA is assumed to initiate the nonstationary energy flow, instead of the selective excitation of the $\nu_s(CH_3)$ modes. These differences make us cautious about the comparison of the results from both MD simulations. Also we notice that the decay of the NMA temperature obtained in Stock et al. work (see Figure 1 in ref 87) slows down as the temperature tends to its equilibrium value. The authors found a 7.7 ps decay time for the slower part of the curve, which roughly corresponds to the temperature involved in our simulations (~400 K). This value is approximately halfway between the experimental relaxation time[47] and the NMAD relaxation time extracted from our simulations. The Stock et al. results seem to indicate that the lower rate of intermolecular VET from the NMAD molecule to the solvent obtained in classical MD simulations is a consequence of the lack of zero-point vibrational energy. If these energies were included in all the vibrational degrees of freedom of the NMAD molecule, the classical result would be expectedly in closer agreement with experiment. Furthermore, the discrepancies between computational and measured rates of energy flow found in our work seem to be comparable to those found in previous studies of different peptides.[16–21]

To find out the role that the solvent plays in the overall relaxation process, we have performed additional simulations using first a rigid model of the solvent obtained by freezing the bending and the stretching internal motions of the D_2O molecules with the SHAKE algorithm.[88] The time evolution of the total NMAD vibrational energy thus obtained is compared in Figure 2 with that provided by the flexible solvent model. As observed, the vibrational relaxation slows down when all of the internal motions of the solvent molecules are frozen, with the relaxation time rising to 15.2 ps. It is quite clear then that the solvent vibrations participate actively in the relaxation
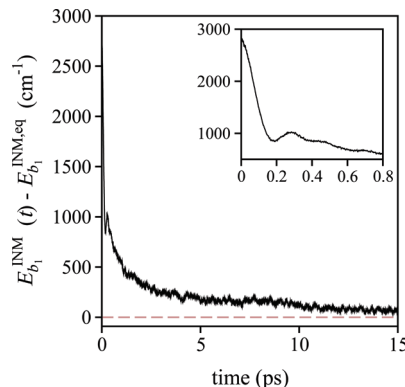
process. Taking into account that the time averaged frequency of the $\nu_s(CH_3)$ modes is ~2843 cm^{-1} (see Table 1), two different relaxation pathways are possible in this respect. The first is an intermolecular vibration-to-vibration (VV) transfer to the stretching modes of the D_2O molecules, which have a measured frequency[83] of $\omega_s = 2500$ cm^{-1}, with the spare energy being deposited in the solvent librational modes, which are centered[89] at $L_1 = 315$ and $L_2 = 520$ cm^{-1} with bandwidths of ≈100 cm^{-1}. The second pathway is the relaxation of the $\nu_s(CH_3)$ modes through a third-order resonance with the bending modes of the D_2O molecules, which have a measured frequency[83] of $\omega_b = 1209.4$ cm^{-1}, and one mid-energy mode of NMAD like the 22nd INM, which has an average frequency of 1615 cm^{-1}. To distinguish between these two intermolecular VV pathways, we have carried out MD simulations using a semirigid model of the solvent in which only the O—D stretching motions are frozen, thus closing the stretching VV relaxation channel. The vibrational energy decay curve resulting from these semirigid simulations is also plotted in Figure 2 and, as observed, is practically identical, within the statistical oscillations, to the decay curve obtained using the flexible model. It means therefore that only the bending modes of the D_2O molecules participate in the vibrational relaxation of the NMAD molecule, with the VV transfer to the stretching modes of the solvent being closed.

3.2. Vibrational Relaxation of the $\nu_s(CH_3)$ Modes. Let us consider specifically now the relaxation of the $\nu_s(CH_3)$ modes. The time evolution of the vibrational energy of these modes is shown in Figure 3. The corresponding decay curve fits well to a triple-exponential function of the form

$$\frac{E_{b_1}^{vib}(t) - E_{b_1}^{vib,eq}}{E_{b_1}^{vib}(0) - E_{b_1}^{vib,eq}} = a_{rel}e^{-t/\tau_{rel}} + a'_{rel}e^{-t/\tau'_{rel}} + a''_{rel}e^{-t/\tau''_{rel}}$$

(7)

where τ_{rel}, τ'_{rel}, and τ''_{rel} are relaxation times, and a_{rel}, a'_{rel}, and a''_{rel} are the corresponding amplitudes that satisfy $a_{rel} + a'_{rel} + a''_{rel} = 1$. The values of these fitting parameters are given in the upper part of Table 2. As observed, the three relaxation times, 0.07, 0.92, and 10.6 ps, are sufficiently separated so as to infer that the whole relaxation process takes place in three different well-defined stages, each one dominated by a given relaxation mechanism. Accordingly, we delimit these three stages roughly by the times $2\tau_{rel} = 0.14$ and $2\tau'_{rel} = 1.84$ ps and analyze them in what follows separately.

3.2.1. First Relaxation Stage (t < 0.14 ps). As already indicated, we have performed all the MD simulations with the

TABLE 2: Fitting Parameters for the Vibrational Relaxation of Different INMs of NMAD, Including Relaxation and Excitation Times (ps), Amplitudes (%), and the Parameter A (cm^{-1})

$E_i^{INM} = a_{rel}e^{-t/\tau_{rel}} + a'_{rel}e^{-t/\tau'_{rel}} + a''_{rel}e^{-t/\tau''_{rel}}$	τ_{rel}	a_{rel}	τ'_{rel}	a'_{rel}	τ''_{rel}	a''_{rel}
group b$_1$ (ν_s(CH$_3$))	0.07	60	0.92	30	10.6	10

$E_i^{INM} = A(a_{rel}e^{-t/\tau_{rel}} + a'_{rel}e^{-t/\tau'_{rel}} - e^{-t/\tau_{exc}})$	τ_{exc}	τ_{rel}	a_{rel}	τ'_{rel}	a'_{rel}	A
group a$_2$ (δ(CH$_3$))	0.07	0.92	50	10.6	50	1422
21st INM (δ_s(NCH$_3$))	0.07	0.92	34	10.6	66	253

$E_i^{INM} = A(e^{-t/\tau_{rel}} - a_{exc}e^{-t/\tau_{exc}} - a'_{exc}e^{-t/\tau'_{exc}})$	τ_{exc}	a_{exc}	τ'_{exc}	a'_{exc}	τ_{rel}	A
group b$_2$ (ν(CH$_3$))	0.07	20	0.92	80	10.6	694
23rd INM (amide I)	0.07	8	0.92	92	10.6	105
22nd INM (amide II)	0.07	12	0.92	88	10.6	191
group a$_1$ (r(CH$_3$) + ν_s(NC))	0.07	10	0.92	90	10.6	628

$E_i^{INM} = A(e^{-t/\tau_{rel}} - e^{-t/\tau_{exc}})$	τ_{exc}	τ_{rel}	A
24th INM (amide A)	2.03	10.6	143
10th INM (amide III)	3.35	10.6	135
9th INM (skel d)	3.35	10.6	140

excess of vibrational energy initially located in the ν_s(CH$_3$) INMs, in keeping with the IR pulse tuned to the CH-stretch transition used in the experiments conducted by Dlott et al.[47] However, the nature of the initial state cannot be considered experimentally as a pure CH-stretch. As pointed out by Dlott et al.,[47] other vibrations are excited during the IR pump pulse through coherent coupling. In our simulations, the initially excited stretching state rapidly evolves into a mixed stretch−bend state by fast energy transfer from the ν_s(CH$_3$) modes to the δ(CH$_3$) modes, in agreement with experimental works[47,59,90–94] that attribute this process to a 2:1 Fermi resonance. The time resolution of the experiments by Dlott et al.[47] is limited by the laser pulse duration of 1.4 ps. In contrast, there is no practical resolution limit in our simulations, so we can directly monitor the fast energy transfer taking place in this very first stage of the relaxation process. In the inset of Figure 3 we see concretely
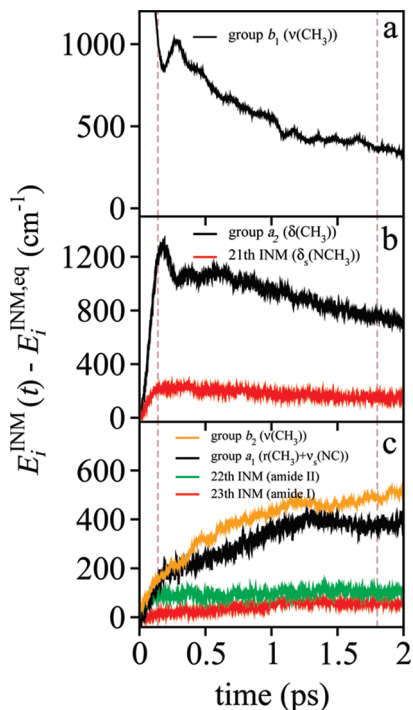

Figure 4. Vibrational energies of the INMs of NMAD that participate in the first and second relaxation stages, relative to their equilibrium values. Vertical dashed lines are placed at 0.14 and 1.84 ps.

how the vibrational energy of the ν_s(CH$_3$) modes drops steeply, with the associated relaxation time of $\tau_{rel} = 0.07$ ps that corresponds to an amplitude of 60% of the total signal. This initial decay is accompanied by a fast increase in the energy of both the bending δ(CH$_3$) modes which form the group a$_2$, and the δ_s(NCH$_3$) bend (21st INM), as clearly shown in Figure 4b where these energies are plotted. The bending modes reach their maxima at ∼0.14 ps, that is, at twice the value of τ_{rel}, and at that time, about 90% of the energy corresponding to this first relaxation channel has abandoned the CH-stretching modes. The maximum energy stored in group a$_2$ and the 21st INM is, respectively, 1300 and 240 cm^{-1}, which account for nearly 75% of the total vibrational energy released by the ν_s(CH$_3$) INMs in this first stage. The rest of the vibrational energy goes essentially to group a$_1$ (150 cm^{-1}), group b$_2$ (150 cm^{-1}), and the 22nd (90 cm^{-1}) and the 23rd (20 cm^{-1}) INMs, as observed in Figure 4c, where the time evolution of the vibrational energy stored in these modes is depicted.

Let us investigate now the mechanisms that control the release of energy from the parent C−H stretches in the first relaxation stage. Previous studies[53–56] based on the use of time-dependent perturbation theory have established that the main relaxation pathways of the amide I mode of the NMAD molecule in liquid heavy water can be accounted for by third-order interactions. Moreover, the anharmonic decay of vibrational modes in the amide I band of myoglobin has been shown to be essentially independent of temperature from below 10 K to over 300 K.[38] These experimental results are in agreement with the independence of the energy transfer rates obtained considering only the contribution of cubic anharmonic potential terms on the temperature.[42,67] This behavior has been reported only for normal modes with frequencies above 500 cm^{-1} which, as seen in Table 1, is the case for most of the NMAD normal modes. We show below that effectively only third-order couplings are necessary to describe the main aspects of the relaxation of the CH-stretching modes.

The viability of a given VER pathway depends, following perturbative arguments,[54–56,62] on two factors. The first one is the resonance condition to be met between the parent mode (P) that releases the energy and the secondary modes α and β that receive that energy. This condition is quantified by the frequency difference $\omega_{P\alpha\beta}(t)$ given by

$$\omega_{P\alpha\beta}(t) = \omega_P(t) - \omega_\alpha(t) - \omega_\beta(t) \qquad (8)$$

TABLE 3: Main Candidates for Resonances in the Vibrational Relaxation of NMAD Excited in the $\nu_s(CH_3)$ Stretches[a]

P	$\alpha + \beta$	$\bar{\omega}_{P\alpha\beta}$	$\Delta\omega_{P\alpha\beta}$	$\bar{G}_{P\alpha\beta}$	$\Delta G_{P\alpha\beta}$	$(\bar{C}_{P\alpha\beta})^{1/2}$
b_1	$a_2 + a_2$	0.5	7.0	0.60	0.28	61.6
b_1	$23 + a_1$	8.3	21.8	1.40	0.62	15.2
b_1	$21 + a_2$	−22.2	35.9	0.76	0.27	12.5
b_1	$22 + a_1$	51.7	47.4	1.69	0.51	9.5
b_1	$24 + 5$	−8.6	20.2	0.20	0.09	3.2
a_2	$a_1 + 4$	0.6	12.5	2.53	1.03	77.9
a_2	$a_1 + 5$	−1.9	10.9	2.75	1.13	76.4
23	$a_1 + 7$	3.3	18.7	7.36	1.83	93.5
b_2	$22 + a_2$	−3.8	14.3	0.95	0.43	92.6
b_2	$21 + a_2$	9.0	27.2	0.97	0.43	74.7
b_2	$a_2 + a_2$	46.6	40.1	0.64	0.37	12.5

[a] Overlined variables denote time averaged values and the Δ symbol stands for standard deviations. Frequencies are given in cm^{-1} and overlaps in $(g/mol)^{3/2}$.

so the smaller the absolute value of this difference, the more efficient the energy transfer. The second factor is the magnitude of the coupling among the three modes involved in the process. Kidera et al.[95,96] have shown that this coupling is highly correlated with the geometrical overlap among the corresponding modes, $G_{P\alpha\beta}$, which can be calculated using the expression

$$G_{P\alpha\beta} = \sum_{i=1}^{N_s} m_i^{3/2} |\mathbf{v}_{i,P}||\mathbf{v}_{i,\alpha}||\mathbf{v}_{i,\beta}| \quad (9)$$

where N_s is the number of atoms in the molecule and $|\mathbf{v}_{i,j}|$ is the absolute value of the 3D vector of the eigenvector component for mode j and atom i. On the basis of the works by Fujisaki et al.,[54–56,62] we identify the dominant VER pathways by means of the Fermi resonance parameter, defined as follows

$$C_{P\alpha\beta} = \left(\frac{G_{P\alpha\beta}}{\omega_{P\alpha\beta}}\right)^2 \quad (10)$$

so that high values of this parameter are expected to result in an increased efficiency of the energy transfer between the modes involved.

In Table 3 we include the time averaged values of $\omega_{P\alpha\beta}$, $G_{P\alpha\beta}$, and $C_{P\alpha\beta}$ for different combinations of INMs, which are the best candidates for resonances in the vibrational relaxation of NMAD after excitation of the $\nu_s(CH_3)$ stretching modes. Note first that the values of $\omega_{P\alpha\beta}(t)$ and $G_{P\alpha\beta}$ show different tendencies so that the values of the Fermi parameter are sometimes driven by an excellent match of the energies but in other cases the strength of the coupling is crucial. For the specific resonances that control the decay of the parent modes in the first relaxation stage, the highest value of the Fermi parameter corresponds, by far, and expectedly, to the 2:1 Fermi resonance that couples the parent b_1 stretching modes with bending modes of the group a_2, in agreement with the large amount of energy accumulated by this a_1 group in the first stage (see Figure 4b). The rest of the relaxation channels of parent b_1 modes are, by decreasing order of importance, $(b_1, 23, a_1)$, $(b_1, 21, a_2)$, $(b_1, 22, a_1)$, and $(b_1, 24, 5)$, and they play a more secondary role in this first stage of the relaxation process, according to the values of their Fermi parameters included in Table 3.

3.2.2. Second Relaxation Stage ($0.14 < t < 1.84$ ps). Once the major part of the excess of vibrational energy initially
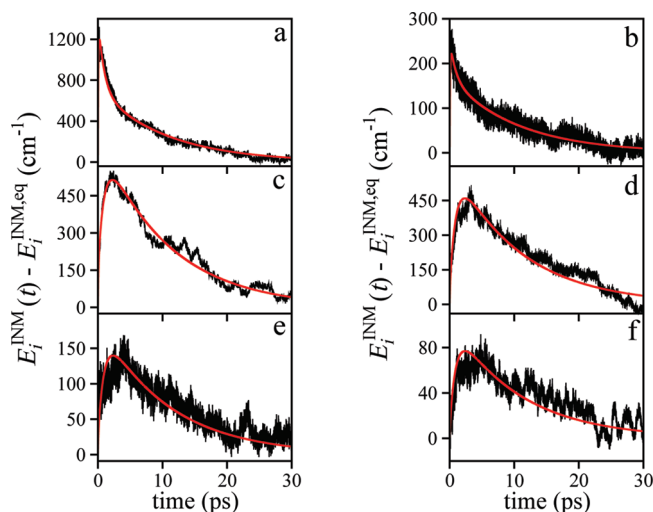

Figure 5. Vibrational energies of assigned INMs of NMAD, relative to their equilibrium values: (a) group a_2 ($\delta(CH_3)$), (b) 21st INM ($\delta_s(NCH_3)$), (c) group b_2 ($\nu(CH_3)$), (d) group a_1 ($r(CH_3) + \nu_s(NC)$), (e) 22nd INM (amide II), and (f) 23rd INM (amide I). Black lines are the results of the simulations, and red lines are the fits to kinetic models (see text).

deposited in the C−H stretches is released during the first ultrashort relaxation stage, the second stage starts to operate from an initial state mainly formed by a combination of group a_2, the 21st INM, and the amount of energy that is still left in the parent group b_1. In Figure 4a,b we see how the vibrational energy in these modes evolves with time along the second relaxation stage, specifically up to 2 ps. To analyze better the time evolution of the intermediate bending modes collected in group a_2 and the 21st INM, we have plotted in Figure 5a,b the vibrational energies of these modes nearly up to completion of the whole relaxation process at 30 ps. These vibrational energies are in turn well reproduced by a function of the type

$$\frac{E_i^{INM}(t) - E_{i,eq}^{INM}}{E_i^{INM}(0) - E_{i,eq}^{INM}} = A(a_{rel}e^{-t/\tau_{rel}} + a'_{rel}e^{-t/\tau'_{rel}} - e^{-t/\tau_{exc}}) \quad (11)$$

which includes, as observed, one exponential excitation term and two exponential relaxation terms. We achieve a good fit to this function by fixing the excitation time τ_{exc} at the relaxation ultrashort time of the parent modes, 0.07 ps, and the relaxation times τ_{rel} and τ'_{rel} at the second and third relaxation times of the parent modes, 0.96 and 10.63 ps, respectively. We leave, therefore, only the weights of the two relaxation channels, a_{rel} and a'_{rel}, which satisfy $a_{rel} + a'_{rel} = 1$, and the A parameter to be fitted. The values obtained for these parameters are included in Table 2, and the curves resulting form the fits are superimposed in Figure 5a,b. The interpretation of these fits indicates then that the $\delta(CH_3)$ bends comprising group a_2 and the 21st INM, act as an energy reservoir of the C−H stretches, becoming excited almost instantaneously in the first stage to then relax jointly during the second and third stages.

The vibrational energy released by the parent b_1 modes, and also by the intermediate a_2 and the 21st INMs, in the second relaxation stage continues to be channelled toward groups b_2 and a_1, and the 22nd and 23rd INMs, as in the first stage, but at a lower rate, as clearly observed in Figure 4b, since the first coherent relaxation channel of the parent group b_1 is now closed. The time evolution of the vibrational energies of all these

intermediate INMs along the entire relaxation process is shown in Figure 5c–f. In agreement with the previous considerations, these energies are reasonably well fitted by the function

$$\frac{E_i^{\text{INM}}(t) - E_{i,\text{eq}}^{\text{INM}}}{E_i^{\text{INM}}(0) - E_{i,\text{eq}}^{\text{INM}}} = A(e^{-t/\tau_{\text{rel}}} - a_{\text{exc}}e^{-t/\tau_{\text{exc}}} - a'_{\text{rel}}e^{-t/\tau'_{\text{rel}}})$$

(12)

which includes two exponential excitation terms, with the excitation times τ_{exc} and τ'_{exc} fixed at the two first relaxation times of the parent modes, 0.07 and 0.92 ps, and one exponential relaxation term, with τ_{rel} fixed at the third relaxation time of the parent modes, 10.6 ps. The weight values of the two excitation channels, a_{exc} and a'_{exc}, and the parameter A for all these intermediate modes are included in Table 2, too, and the corresponding fits are plotted in Figure 5c–f.

The channels that control the excitation of the intermediate modes in the second stage can be rationalized again in terms of the Fermi parameter given by eq 10. Effectively, we see in Table 3 that there are two secondary channels mediated by the resonances, $(a_2, a_1, 4)$ and $(a_2, a_1, 5)$, which facilitate the relaxation of group a_2 of modes $\delta(\text{CH}_3)$ by exciting group a_1 formed by the $r(\text{CH}_3)$ and $\nu_s(\text{NC})$ modes. This pathway explains our finding of a common value for the first relaxation time of the group a_2 modes and the second excitation time of the a_1 modes. We note that these types of relaxation pathways have already been reported in other systems.[91,97] Moreover, we have the $(23, a_1, 7)$ resonance, which is also quite strong and favors the rapid dissipation of the vibrational energy deposited in the 23rd INM through the $(b_1, 23, a_1)$ pathway to the a_1 group, thus explaining why the 23rd INM stores less energy, nearly half, than the 22nd INM, as observed in Figure 5e,f.

The excitation of the INMs of group b_2, which have vibrational frequencies higher than the parent b_1 modes, is a pure classical effect without quantum counterpart, which has been already reported in other classical simulations.[56,57,95,96,98] In our case, this unrealistic excitation takes place essentially through the third-order resonances $(b_2, 21, a_2)$ and $(b_2, 22, a_2)$, with a much lesser contribution from the weaker resonance (b_2, a_2, a_2) (see Table 3). As observed in Figure 5c, the amount of energy stored in the b_2 modes is almost 500 cm^{-1}. When distributed in the four modes comprising this group, this energy accounts for ~4% of the population of each mode. Since the population of the modes is the quantity directly measured (see subsection 3.3 below), we think that this unphysical classical energy transfer has only a residual effect on the entire relaxation process.

3.2.3. Third Relaxation Stage (t > 1.84 ps). During the third relaxation stage, all of the previously excited high and mid-frequency modes, that is, groups b_1, b_2, a_1, and a_2 and the 21st, 22nd, and 23rd INMs, relax toward equilibrium with the common third stage relaxation time of 10.6 ps. In addition, we find that the low-frequency 9th (skel d), 10th (amide III), and 24th (amide A) INMs also relax at the same rate. In Figure 6 we plot the time evolution of these three modes along the whole relaxation process. Their vibrational energies are now fitted to the exponential excitation-plus-relaxation function

$$\frac{E_i^{\text{INM}}(t) - E_{i,\text{eq}}^{\text{INM}}}{E_i^{\text{INM}}(0) - E_{i,\text{eq}}^{\text{INM}}} = A(e^{-t/\tau_{\text{rel}}} - e^{-t/\tau_{\text{exc}}})$$
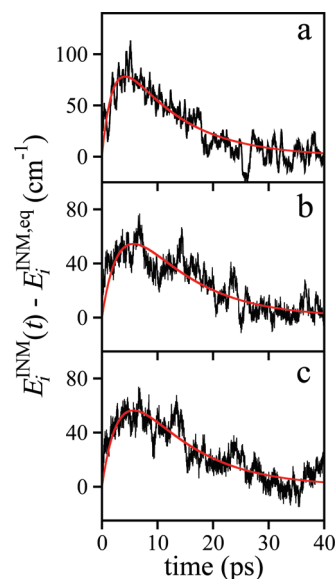
(13)

Figure 6. Vibrational energies of the assigned INMs of NMAD relative to their equilibrium values: (a) 24th INM (amide A), (b) 10th INM (amide III), and (c) 9th INM (skel d). Black lines are the results of the simulations, and red lines are the fits to kinetic models (see text).

TABLE 4: Fitting Parameters of the Vibrational Relaxation of the $\nu_s(\text{CH}_3)$ Stretches of NMAD Resulting from the Different Sets of MD Simulations[a]

$E_i^{\text{INM}} = a_{\text{rel}}e^{-t/\tau_{\text{rel}}} + a'_{\text{rel}}e^{-t/\tau'_{\text{rel}}} + a''_{\text{rel}}e^{-t/\tau''_{\text{rel}}}$		τ_{rel}	a_{rel}	τ'_{rel}	a'_{rel}	τ''_{rel}	a''_{rel}
group b_1 ($\nu_s(\text{CH}_3)$)	flexible solvent	0.07	60	0.92	30	10.6	10
	semirigid solvent	0.07	60	0.92	30	10.7	10
	rigid solvent	0.07	60	0.92	30	14.2	10
	in vacuo	0.07	70	1.93	30		

[a] Relaxation and excitation times are in picoseconds, and amplitudes in percent.

with the relaxation time τ_{rel} fixed to 10.6 ps. The results from these fits are included in Table 2. As observed, the 9th, 10th, and 24th modes are excited at lower rates than the other intermediate modes ($\tau_{\text{exc}} \sim 3$ ps) and therefore reach their maxima at longer times (~5 ps). The low-frequency 9th and 10th INMs are presumably excited by relaxation of previously excited mid-energy modes. As for the high-frequency 24th INM, it receives its energy from the parent b_1 modes, with the spare energy going to the water solvent librations. We have checked this by carrying out simulations in the absence of the solvent, in which it is observed that the 9th and 10th INMs continue to be excited, while the 24th INM does not.

3.3. Role of the Solvent in the Relaxation Process. Let us consider now the effect of the solvent on each of the relaxation stages described previously. For this purpose we use the nonequilibrium MD simulations carried out using the semirigid (OD distances frozen) and rigid solvent models, and the in vacuo simulations. Concretely, we have fitted the vibrational relaxation of the parent $\nu_s(\text{CH}_3)$ modes from these simulations to the triple-exponential function given by eq 7. The results from these fits together with those corresponding to the flexible solvent model are collected in Table 4. We note that the exponential amplitudes in the semirigid and rigid fits are set equal to the corresponding amplitudes of the flexible model fit.

The times included in Table 4 show that the first relaxation time τ_{rel} associated with the coherent ultrafast energy transfer from the parent $\nu_s(\text{CH}_3)$ modes to the $\delta(\text{CH}_3)$ modes maintains the same value of 0.07 ps in all the simulations. This confirms that the first relaxation stage is a purely IVR process, with no
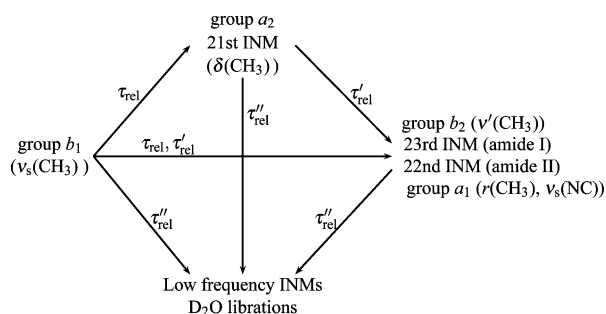
Figure 7. Kinetic scheme for the relaxation of NMAD in liquid deuterated water after C−H stretch excitation, based on a three-stage relaxation model.

Figure 8. Population of the group b_1 ($\nu_s(CH_3)$) modes: simulated (red line) and experimental (closed squares) results. The results from the simulations have been transformed through a Gaussian convolution with fwhm = 1.4 ps.

energy dissipated into the bath. The second relaxation time τ'_{rel} = 0.92 ps is affected neither by the partial nor by the total freezing of the internal motions of the solvent. Its value rises noticeably, however, up to 1.93 ps in the in vacuo simulations, which is an indication that the solvent librations participate in the second stage of the relaxation process. Finally, and expectedly, we see in Table 4 that the internal motions of the solvent play a more important role in the third relaxation stage. Although the longest relaxation time for the flexible model of the solvent, τ''_{rel} = 10.6 ps, hardly changes when the water OD stretches are frozen, it rises up to 14.2 ps when the bend angle is, additionally, fixed, meaning that the third relaxation stage slows down quite significantly in this case. In passing, we note that this slow down is also observed in the relaxation of the intermediate INMs previously excited by IVR. We also see in Table 4 that the third relaxation stage does not occur in the absence of the solvent. From all this we conclude that the third stage proceeds essentially through intermolecular VET to the librations of the solvent and, to a lesser extent, to the solvent bends. Interestingly, the values of τ''_{rel} obtained using a flexible or a rigid solvent model (10.6 and 14.2 ps, respectively) are only slightly smaller than the vibrational relaxation time of the NMAD molecule obtained in the same conditions (11.7 and 15.2 ps). This fact probes that this process is the limiting step of the relaxation of the NMAD molecule. In Figure 7 we depict a kinetic scheme that summarizes the relaxation process of NMAD in liquid deuterated water after excitation of the C−H stretches, as rationalized by the three-stage model proposed.

3.4. Comparison with Experiments. After analyzing the results from the nonequilibrium MD simulations of the $\nu_s(CH_3)$ vibrational relaxation, we compare them with the experimental data obtained by Dlott et al.[47] by ultrafast time-resolved infrared-Raman spectroscopy. In their experiments, they measure the time evolution of the populations of the vibrational modes. Accordingly, we have evaluated the populations $n_i(t)$ of the INMs from the simulation as follows

$$n_i(t) = \frac{E_i^{INM}(t)}{\hbar\omega_i(t)} \qquad (14)$$

where $\omega_i(t)$ are INM frequencies. This expression is clearly an approximation to calculate quantum-like populations from classical simulations in which the energy is not quantized and there is not zero-point vibrational energy.

Before going into the comparison with experiments, it is convenient to recall that the intermediate relaxation modes of medium size molecules like NMAD can be roughly divided, according to the seminal work by Nitzan and Jortner,[99] in mid-
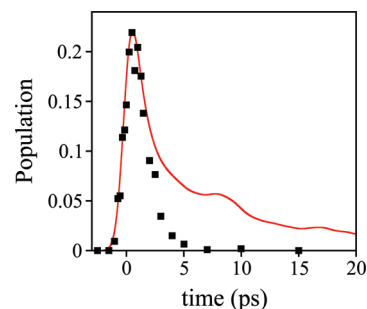
range-energy modes M, and lower-energy modes L. Typically, the mid-range modes have a strong harmonic character with frequencies in the 1700−1200 cm^{-1} range, and the lower modes are more anharmonic vibrations with frequencies below 1200 cm^{-1}. For NMAD, the INMs analysis shows then (see Table 1) that the 1st to 15th INMs are L modes, and the 16th to 24th INMs are M modes. This classification is based on the three-stage model used by Dlott et al.[47] to explain the experimental data of the vibrational relaxation of the $\nu_s(CH_3)$ modes of NMAD. In this mode, the first stage is the relaxation of the parent (P) or initially excited states to M and L vibrations via IVR, without a significant energy dissipation to the solvent. In the second stage, the excited M vibrations decay by exciting L vibrations plus the bath, while the L vibrations decay by exciting the bath only. In the third stage, the remaining L excitations decay into the bath. The model assumes that all vibrations belonging to the same level have the same lifetime.

In Figure 8 we plot the population of the parent $\nu_s(CH_3)$ modes obtained from the simulations along with the experimental ones. To make a proper comparison of them, we have scaled the experimental populations by a factor of 7.65 by matching its maximum with the peak height of the theoretical populations. This scaling has also been applied to the rest of mid-range and low-frequency modes for the sake of data consistency. We see first in Figure 8 that the coherent ultrashort relaxation of the parent modes (τ_{rel} = 0.07 ps) does not show up, since it is masked by the 1.4 ps Gaussian convolution applied to the simulation results to mimic the infrared laser pulse duration. The theoretical and experimental $\nu_s(CH_3)$ populations agree quite well up to about 2 ps, that is, until the second relaxation time is over, and deviate significantly from this time on, during the third relaxation stage, in which the simulations exhibits a much slower decay. The relaxation time associated with our second relaxation stage, τ'_{rel} = 0.92 ps, is in fact quite close to the relaxation time of the parent modes provided by Dlott et al.[47] of 1.2(±0.2) ps, but our third relaxation time, τ''_{rel} = 10.6 ps, is considerably longer than the mid-range and low-frequency decay times, 1.7(±0.2) and 2.8(±0.5) ps, reported by Dlott et al. Accordingly, our simulations reproduce well the relaxation of the parent to the mid-range modes, which accounts for ∼90% of the total energy deposited initially in the parent modes but provides a noticeably slower dissipation of the vibrational energy into the low-frequency modes and the bath.

In Figure 9 we compare the simulation and experimental populations of the mid-range modes that participate in the whole relaxation process. Experimentally, the highest mid-range excitation corresponds to the amide II (24th INM) mode. In contrast, the mid-range INMs that populate most in the simulations are the bending $\delta_a(CCH_3)$ modes that form group

C−H Stretching Modes of *N*-methylacetamide-*d*

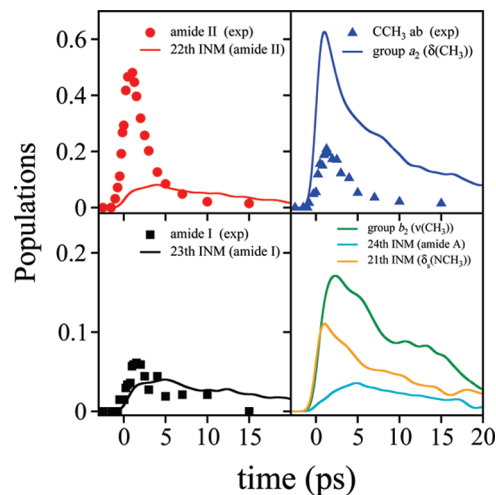*J. Phys. Chem. A, Vol. 114, No. 43, 2010* **11459**

Figure 9. Populations of the mid-range (*M*) frequency INMs. The experimental data are represented by symbols, and the results of the simulations are drawn with lines. The results from the simulations have been transformed through a Gaussian convolution with fwhm = 1.4 ps.
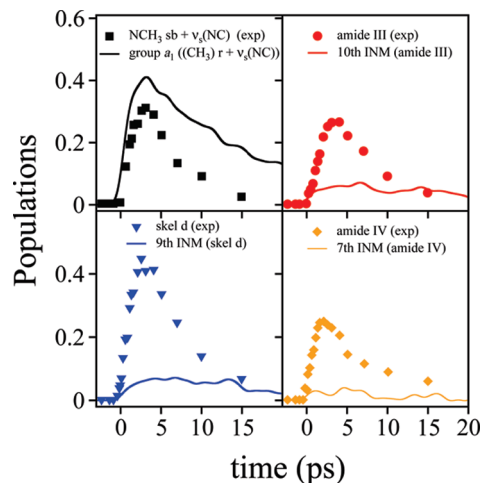

Figure 10. Populations of the low (*L*) frequency INMs. The experimental data are represented by symbols, and the results of the simulations are drawn with lines. The results from the simulations have been transformed through a Gaussian convolution with fwhm = 1.4 ps.

a_2. In both cases, the energy transfer to the corresponding M modes is mediated by a strong 2:1 Fermi resonance with the parent $\nu_s(CH_3)$ modes. The discrepancy in which the mid-range mode couples to the parent mode lies in the differences existing between the experimental and the calculated frequencies of these three modes. While the experimental frequencies of the parent C−H stretches and the amide II mode, 2945 and 1490 cm^{-1} respectively, justify the Fermi 2:1 resonance between these modes, in the simulations the averaged frequency of the parent $\nu_s(CH_3)$ INMs is 2843.6 cm^{-1} (see Table 1) and, as discussed above (see Table 3), they couple through a 2:1 Fermi to the $\delta_a(CCH_3)$ bends of group a_2, which have an averaged INM frequency of 1401.8 cm^{-1} (see Table 1). The nonuniform accuracy of the generic AMBER force field in the calculation of the frequencies of the different INMs[48] affects the prediction of the relative strength that the IVR pathways have in the VER process. Previous works[59,93,94] show that our results are in agreement with the typical relaxation of the $\nu_s(CH_3)$ modes through the bending $\delta(CH_3)$ modes.

Besides the excitations of the amide II and the $\delta_a(CCH_3)$ modes, the excitation of the amide I (23th INM) mode is also observed experimentally, although in a much weaker way, in agreement with our simulation results (see Figure 9). In addition, the MD simulations provide excitations of the $\delta_s(NCH_3)$ (21st INM), amide A (24th INM), and $\nu'(CH_3)$ (group b_2) modes (see Figure 9), which are not detected experimentally.

The populations of the low-frequency L modes are shown in Figure 10. The vibrational modes observed experimentally by Dlott et al.[47] in this case are the $\delta_s(NCH_3)$ bend, the $\nu_s(NC)$ stretch, the amide III, the skel d, and the amide IV. In our simulations, the $\nu_s(NC)$ mode belongs to group a_1, and amide III, skel d, and amide IV identify with the 10th, 9th, and 7th INMs, respectively.

Concerning the $\delta_s(NCH_3)$ mode we note that Dlott et al.[47] assign the observed frequency of 1192 cm^{-1} to it, while the original work of Krimm et al.[100] assigns it to a much higher frequency of 1412 cm^{-1}. In our analysis the $\delta_s(NCH_3)$ mode nominally belongs to the mid-range a_2 group, with an INM frequency of 1400.5 cm^{-1} (see Table 1), in agreement with the experimental assignment provided by Krimm et al.[100] Also in the work by Krimm et al., the range of frequencies between 1125 and 1185 cm^{-1} is associated with the in-plane rock and

the out-of-plane rocking motions of the methyl groups, which correspond to group a_1 in our simulations. Accordingly, in our comparison with the experimental data, we consider the $\delta_s(NCH_3)$ mode as an a_2 mode. Except for the high theoretical population achieved by group a_1, the maximum populations observed in the L modes are significantly larger than those obtained in our simulations. The main discrepancy is found in the excitation of the 7th INM (amide IV). While this state is only slightly excited during our simulations, a significant excitation is observed experimentally. This difference could be attributed to the higher experimental excitation of the amide II mode, since this mode presents a Fermi resonance with the combination mode of amide IV and the skel d mode. It is worth noting that, according to the experimental data, the L modes remain significantly populated after 15 ps, which seems to be contradictory to the NMAD vibrational relaxation time of 5.1 ps observed.[47]

Finally, our results can be analyzed in terms of the scheme proposed by Nitzan and Jortner,[90,99] in which three energy regimes are expected for VER. The first regime corresponds to the lowest frequency vibrations with short lifetimes due to their strong coupling with the bath. Our simulations do not show significant excitations of the 1st to 4th INMs, while the populations of the 5th to 8th INMs reach maximum values below 5%. Nevertheless, the 4th and 5th INMs participate in third-order resonance channels in which the mid-range vibrations relax (see Table 3). The relevance of these channels has been verified by performing molecular dynamics simulations freezing these two INMs. We have thus found (results not shown) that the relaxation of the group a_2 and the excitation of the group a_1 slow down when the 4th and 5th INMs are frozen. Moreover, the energy stored in group a_1 decreases, which demonstrates the relevance of the relaxation channel in which the a_2 modes transfer their excess of vibrational energy through resonances to the a_1 modes and the 4th and 5th INMs. The lack of excitation of the 4th and 5th INMs during simulations without constraints can be attributed to a fast intermolecular energy transfer between these modes and the solvent librations. A similar behavior was found in our study for the amide I mode.[57] The second Nitzan and Jortner regime corresponds to intermediate energy vibrations with longer lifetimes, due to the limited number of relaxation channels open for these modes to transfer their energy to the

lower-energy vibrations and the solvent. Our simulations show that the mid-range modes present a significant accumulation of their excess of vibrational energy during the relaxation process, evidencing faster excitation rates than the relaxation ones. Finally, the third regime includes the high-energy vibrations with short lifetimes, due to the existence of a significant number of states to which the energy can be transferred. Our simulations show that the initially excited parent b_1 modes transfer a large amount of their excess of vibrational energy through an ultrafast coherent process that involves coupling with the a_2 modes and the 23rd INM.

4. Conclusions

In this work we have carried out nonequilibrium MD simulations assisted by INMs analysis to study the photoexcitation and subsequent vibrational relaxation of the C−H stretching vibrations of deuterated *N*-methylacetamide in aqueous (D_2O) solution. The methodology employed allows us to assign unequivocally each INM to an individual ENM, or to a group of ENMs. In this way, the variation in time of the excess of vibrational energy for all the assigned INMs can be analyzed and compared with time-resolved infrared-Raman spectroscopic measurements. Also, by performing different MD simulations including those using flexible, semirigid or rigid solvent models, and in vacuo simulations, we have been able to characterize the specific IVR and intermolecular VET relaxation pathways. The results are also supported by the analysis of resonances and couplings among the states involved in the process.

According to the energetic and kinetic analysis of the MD simulations, the three-stage kinetic model for the VER of the $\nu_s(CH_3)$ modes of the NMAD in D_2O, which is depicted in Figure 7, has been proposed. We have shown that the time evolution of the excitation and relaxation of the different INMs of the solute can be well reproduced in terms of the three relaxation times included in the model. Also this kinetic scheme agrees reasonably well with the three-stage model proposed by Dlott et al.[47] on the basis of the division of the vibrations of the solute molecule into three tiers: the parent P, the mid-range modes M, and the lower energy modes L.

During the first stage of the relaxation, the parent modes relax in an ultrashort time scale populating different $\delta(CH_3)$ modes. As a result, the initial state after this ultrashort process can be considered as a mixed stretch−bend state in agreement with experiments.[47,59,90–94] Due to the laser pulse duration, this process cannot be observed directly.[47] Next, the stretch−bend modes relax during the second stage with a common biexponential decay through channels that essentially populate different M and L modes. The third stage is dominated by the energy transfer to low frequency modes and to the librations of the solvent. This last stage is the rate limiting process of the relaxation mechanism. In fact, the relaxation time for the total vibrational energy of the molecule of 11.7 ps is only slightly longer than the relaxation time corresponding to this stage of $\tau''_{rel} = 10.6$ ps. We note that this is the main kinetic discrepancy between our model and the experimental findings. Our molecular relaxation time is approximately twice that measured by Dlott et al.[47] of $\tau = 5.1$ ps. In contrast, the relaxation time of the parent modes obtained in our simulations, $\tau'_{rel} = 0.92$ ps, compares well with the experimental values of 1.2($\pm$0.2) ps.[47] As for the role played by vibrational modes of the solvent, we have shown that they participate only in the third, and slowest, relaxation stage through an intermolecular VET to the bending modes of the D_2O molecules.

In relation to the identity of the excited M and L vibrations in the experiments and our simulations, we have found significant differences in the relative excitation amplitudes. The main discrepancy concerns the modes that are initially populated coherently. In the experiments[47] it is the amide II mode that couples to the parent C−H stretching modes, whereas in the simulations it is the $\delta(CH_3)$ modes that enter in resonance with the parent modes. This is due to the nonuniform accuracy of the generic AMBER force field in the calculation of the frequencies of the different normal modes,[48] a fact that clearly affects the prediction of the relative strength that the IVR pathways have on the VER process.

We consider finally that the nonequilibrium MD simulations plus INM analysis method used in this work is a valuable tool to simulate, analyze, and interpret the experiments on the basis of the use of time-resolved infrared-Raman spectroscopies. The main limitations in this respect come from the use of approximate potential energy functions that can alter the resonances driving the relaxation channel and the use of the classical description for the mid-range and, especially, the high-energy vibrational modes, which erases potential quantum effects. In this respect it is worth noticing that a recent study[101] has proposed a method to predict quantum correction factors that connect the results of the classical simulations to match the correct quantum results. Work along these two lines is currently in progress in our group.

References and Notes

(1) Sagnella, D. E.; Straub, J. E. *Biophys. J.* **1999**, *77*, 70–84.
(2) Bu, L.; Straub, J. E. *Biophys. J.* **2003**, *85*, 1429–1439.
(3) Kern, D.; Zuiderweg, E. R. P. *Curr. Opin. Struct. Biol.* **2003**, *13*, 748–757.
(4) Guallar, V.; Jarzecki, A. A.; Friesner, R. A.; Spiro, T. G. *J. Am. Chem. Soc.* **2006**, *128*, 5427–5435.
(5) Kubo, M.; Shiomitsu, E.; Odai, K.; Sugimoto, T.; Suzuki, H.; Ito, E. *J. Mol. Struct.* **2003**, *639*, 117–128.
(6) Pouthier, V. *J. Chem. Phys.* **2008**, *128*, 065101.
(7) Wang, Z.; Pakoulev, A.; Dlott, D. *Science* **2002**, *296*, 2201–2203.
(8) Gruebele, M.; Wolynes, P. *Acc. Chem. Res.* **2004**, *37*, 261–267.
(9) Ota, N.; Agard, D. A. *J. Mol. Biol.* **2005**, *351*, 345–354.
(10) Leitner, D. M.; Straub, J. E. *Proteins: energy, heat and signal flow*; CRC Press: Boca Raton, FL, 2009.
(11) Yu, X.; Leitner, D. M. *J. Chem. Phys.* **2005**, *122*, 054902.
(12) Leitner, D. M. Heat transport in molecules and reaction kinetics: The role of quantum energy flow and localization. In *Geometric structures of phase space in multidimensional chaos: A special volume of Advances in Chemical Physics, part B, volume 130*; Toda, M., Komatsuzaki, T., Konishi, T., Berry, R. S., Rice, S. A., Eds.; John Wiley & Sons: New York, 2005; pp 205−256.
(13) Leitner, D. M.; Gruebele, M. *Mol. Phys.* **2008**, *106*, 433.
(14) Fujiwara, H.; Terazima, M.; Kimura, Y. *Chem. Phys. Lett.* **2008**, *454*, 218–222.
(15) Schröder, C.; Vikhrenko, V.; Schwarzer, D. *J. Phys. Chem. A* **2009**, *113*, 14039–14051.
(16) Botan, V.; Backus, E. H. G.; Pfister, R.; Moretto, A.; Crisma, M.; Toniolo, C.; Nguyen, P. H.; Stock, G.; Hamm, P. *Proc. Natl. Acad. Sci. U.S.A.* **2007**, *104*, 12749–12754.
(17) Backus, E. H. G.; Nguyen, P. N.; Botan, V.; Pfister, R.; Moretto, A.; Crisma, M.; Toniolo, C.; Stock, G.; Hamm, P. *J. Phys. Chem. B* **2008**, *112*, 9091–9099.
(18) Nguyen, P. H.; Derreumaux, P.; Stock, G. *J. Phys. Chem. B* **2009**, *113*, 9340–9347.
(19) Schade, M.; Hamm, P. *J. Chem. Phys.* **2009**, *131*, 044511.
(20) Schade, M.; Moretto, A.; Crisma, M.; Toniolo, C.; Hamm, P. *J. Phys. Chem. B* **2009**, *113*, 13393–13397.

(21) Nguyen, P. H.; Park, S.; Stock, G. *J. Chem. Phys.* **2010**, *132*, 025102.

(22) Lockless, S. W.; Ranganathan, R. *Science* **1999**, *286*, 295–299.

(23) Laubereau, A.; Kaiser, W. *Rev. Mod. Phys.* **1978**, *50*, 607.

(24) Miller, R. J. D. *Annu. Rev. Phys. Chem.* **1991**, *42*, 581.

(25) Mizutani, Y.; Kitagawa, T. *Science* **1997**, *278*, 443.

(26) Hamm, P.; Lim, M. H.; Hochstrasser, R. M. *J. Phys. Chem. B* **1998**, *102*, 6123–6138.

(27) Dlott, D. *Chem. Phys.* **2001**, *266*, 149.

(28) Zanni, M. T.; Asplund, M. C.; Hochstrasser, R. M. *J. Chem. Phys.* **2001**, *114*, 4579–4590.

(29) Fayer, M. D. *Annu. Rev. Phys. Chem.* **2001**, *52*, 315.

(30) Woutersen, S.; Hamm, P. *J. Phys.: Condens. Matter* **2002**, *14*, R1035.

(31) Nagy, A. M.; Prokhorenko, V. I.; Miller, R. J. D. *Curr. Opin. Struct. Biol.* **2006**, *16*, 654.

(32) DeFlores, L. P.; Ganim, Z.; Ackley, S. F.; Chung, H. S.; Tokmakoff, A. *J. Phys. Chem. B* **2006**, *110*, 18973–18980.

(33) Wang, Z. H.; Carter, J. A.; Lagutchev, A.; Koh, Y. K.; Seong, N.-H.; Cahill, D. G.; Dlott, D. D. *Science* **2007**, *317*, 787.

(34) Hamm, P.; Helbing, J.; Bredenbeck, J. *Annu. Rev. Phys. Chem.* **2008**, *59*, 291.

(35) Fayer, M. D. *Ultrafast infrared and Raman spectroscopy*; Marcel Dekker Inc.: Amsterdam, 2001.

(36) Mukamel, S.; Hochstrasser, R. *Chem. Phys.* **2001**, *266*, 135–351.

(37) Moran, A. M.; Mukamel, S.-M. P. S. *J. Chem. Phys.* **2003**, *118*, 9971.

(38) Peterson, K. A.; Rella, C. W.; Engholm, J. R.; Schwettman, H. A. *J. Phys. Chem. B* **1999**, *103*, 557–561.

(39) Xie, A.; van der Meer, L.; Hoff, W.; Austin, R. *Phys. Rev. Lett.* **2000**, *84*, 5435.

(40) Austin, R.; Xie, A.; van der Meer, L.; Redlich, B.; Lindgard, P.; Frauenfelder, H.; Fu, D. *Phys. Rev. Lett.* **2005**, *94*, 128101.

(41) Woutersen, S.; Mu, Y.; Stock, G.; Hamm, P. *Proc. Natl. Acad. Sci. U.S.A.* **2001**, *98*, 11254.

(42) Yu, X.; Leitner, D. M. *J. Phys. Chem. B* **2003**, *107*, 1698–1707.

(43) Zanni, M. T.; Asplund, M. C.; Hochstrasser, R. M. *J. Chem. Phys.* **2001**, *114*, 4579–4590.

(44) Woutersen, S.; Pfister, R.; Hamm, P.; Mu, Y.; Kosov, D. S.; Stock, G. *J. Chem. Phys.* **2002**, *117*, 6833–6840.

(45) Rubtsov, I. V.; Wang, J.; Hochstrasser, R. M. *J. Phys. Chem. A* **2003**, *107*, 3384–3396.

(46) DeCamp, M. F.; DeFlores, L.; McCracken, J. M.; Tokmakoff, A.; Kwac, K.; Cho, M. *J. Phys. Chem. B* **2005**, *109*, 11016–11026.

(47) Fang, Y.; Shigeto, S.; Seong, N.; Dlott, D. *J. Phys. Chem. A* **2009**, *113*, 75–84.

(48) Gregurick, S. K.; Chaban, G. M.; Gerber, R. B. *J. Phys. Chem. A* **2002**, *106*, 8696–8707.

(49) Nguyen, P. H.; Stock, G. *J. Chem. Phys.* **2003**, *119*, 11350–11358.

(50) Kwac, K.; Cho, M. *J. Chem. Phys.* **2003**, *119*, 2247–2255.

(51) Schmidt, J. R.; Corcelli, S. A.; Skinner, J. L. *J. Chem. Phys.* **2004**, *121*, 8887–8896.

(52) Hayashi, T.; Zhuang, W.; Mukamel, S. *J. Phys. Chem. A* **2005**, *109*, 9747–9759.

(53) Fujisaki, H.; Zhang, Y.; Straub, J. E. *J. Chem. Phys.* **2006**, *124*, 144910.

(54) Fujisaki, H.; Yagi, K.; Hirao, K.; Straub, J. E. *Chem. Phys. Lett.* **2007**, *443*, 6–11.

(55) Fujisaki, H.; Stock, G. *J. Chem. Phys.* **2008**, *129*, 134110.

(56) Fujisaki, H.; Yagi, K.; Straub, J. E.; Stock, G. *Int. J. Quantum Chem.* **2009**, *109*, 2047–2057.

(57) Bastida, A.; Soler, M. A.; Zúñiga, J.; Requena, A.; Kalstein, A.; Fernandez-Alberti, S. *J. Chem. Phys.* **2010**, *132*, 224501.

(58) Oxtoby, D. W. *Adv. Chem. Phys.* **1979**, *40*, 1–48.

(59) Oxtoby, D. W. *Adv. Chem. Phys.* **1981**, *47*, 487–519.

(60) Rey, R.; Hynes, J. T. *J. Chem. Phys.* **1998**, *108*, 142–153.

(61) Li, S.; Thompson, W. H. *Chem. Phys. Lett.* **2005**, *405*, 304–309.

(62) Zhang, Y.; Fujisaki, H.; Straub, J. E. *J. Phys. Chem. A* **2009**, *113*, 3051–3060.

(63) Nishikawa, T.; Go, N. *Struct. Funct. Genet.* **1987**, *2*, 308.

(64) Brooks, B. R.; Karplus, M. *Proc. Natl. Acad. Sci. U.S.A* **1983**, *80*, 6571.

(65) McCammon, J. A.; Harvey, S. C. *Dynamics of Proteins and Nucleic Acids*; Cambridge University Press: Cambridge, U.K., 1987.

(66) Brooks, B. R.; Karplus, M.; Pettitt, B. M. *Adv. Chem. Phys.* **1988**, *71*, 1.

(67) Leitner, D. M. *Phys. Rev. Lett.* **2001**, *87*, 188102.

(68) Raff, L. M. *J. Chem. Phys.* **1988**, *89*, 5680–5691.

(69) Kabadi, V. N.; Rice, B. M. *J. Phys. Chem. A* **2004**, *108*, 532–540.

(70) Buchner, M.; Ladanyi, B.; Stratt, R. M. *J. Chem. Phys.* **1992**, *97*, 8522–8535.

(71) Keyes, T. *J. Phys. Chem. A* **1997**, *101*, 2921–2930.

(72) Stratt, R. M. The molecular mechanism behind the vibrational population relaxation of small molecules in liquids. In *Ultrafast infrared and Raman spectroscopy*; Fayer, M. D., Ed.; Marcel Dekker Inc.: Amsterdam, 2001; pp 149−190.

(73) Kalstein, A.; Fernández-Alberti, S.; Bastida, A.; Soler, M.; Farag, M. H.; Zúñiga, J.; Requena, A. Submitted for publication.

(74) Wang, Z.; Pang, Y.; Dlott, D. D. *Chem. Phys. Lett.* **2004**, *397*, 40.

(75) Wang, Z.; Pang, Y.; Dlott, D. D. *J. Phys. Chem. A* **2007**, *111*, 3196.

(76) Shigeto, S.; Dlott, D. D. *Chem. Phys. Lett.* **2007**, *447*, 134–139.

(77) Frauenfelder, H.; Sligar, S. G.; Wolynes, P. G. *Science* **1991**, *254*, 1598–1603.

(78) Frauenfelder, H.; Bishop, A. R.; Garcia, A.; Perelson, A.; Schuster, P.; Sherrington, D.; Swart, P. J. *Landscape Paradigms in Physics and Biology: Concepts, Structures, and Dynamics*; North-Holland: Amsterdam, 1997.

(79) Carpaneto, G.; Martello, S.; Toth, P. *Ann. Operations Res.* **1988**, *13*, 193–223.

(80) Nakamura, M.; Tamura, K.; Murakami, S. *Thermochim. Acta* **1995**, *253*, 127–136.

(81) Cornell, W. D.; Cieplak, P.; Bayly, C. I.; Gould, I. R.; K. M. Merz, J.; Ferguson, D. M.; Spellmeyer, D. C.; Fox, T.; Caldwell, J. W.; Kollman, P. A. *J. Am. Chem. Soc.* **1995**, *117*, 5179–5197.

(82) MacKerell, A. D. J.; et al. *J. Phys. Chem. B* **1998**, *102*, 3586–3616.

(83) Venyaminov, S. Y.; Prendergast, F. G. *Anal. Biochem.* **1997**, *248*, 234–245.

(84) Pappu, R. V.; Hart, R. K.; Ponder, J. W. *J. Phys. Chem. B* **1998**, *102*, 9725–9742.

(85) Svanberg, M. *Mol. Phys.* **1997**, *92*, 1085.

(86) Berendsen, H. J. C.; Postma, J. P. M.; van Gunsteren, W. F.; DiNola, A.; Haak, J. R. *J. Chem. Phys.* **1984**, *81*, 3684.

(87) Park, S.; Nguyen, P. H.; Stock, G. *J. Chem. Phys.* **2009**, *131*, 185503.

(88) Ryckaert, J. P.; Ciccotti, G.; Berendsen, H. J. C. *J. Comput. Phys.* **1977**, *23*, 327–341.

(89) Zelsmann, H. R. *J. Mol. Struct.* **1995**, *350*, 95–114.

(90) Déak, J. C.; Iwaki, L. K.; Dlott, D. D. *J. Phys. Chem. A* **1998**, *102*, 8193–8201.

(91) Déak, J. C.; Iwaki, L. K.; Dlott, D. D. *J. Phys. Chem. A* **1999**, *103*, 971–979.

(92) Déak, J. C.; Iwaki, L. K.; Dlott, D. D. *J. Raman. Spectrosc.* **2000**, *31*, 263–274.

(93) Alfano, R. R.; Shapiro, S. L. *Phys. Rev. Lett.* **1972**, *29*, 1655–1658.

(94) Seilmeier, A.; Kaiser, W. Ustrashort intramolecular and intermolecular vibrational energy transfer of polyatomic molecules in liquids. In *Ultrashort laser pulses and applications*; Kaiser, W., Ed.; Springer-Verlag, Berlin: 1988; Vol 60, p 279.

(95) Moritsugu, K.; Miyashita, O.; Kidera, A. *Phys. Rev. Lett.* **2000**, *85*, 3970–3973.

(96) Moritsugu, K.; Miyashita, O.; Kidera, A. *J. Phys. Chem. B* **2003**, *107*, 3309–3317.

(97) Iwaki, L.; Dlott, D. D. Vibrational energy transfer in condensed phases. In *Encyclopedia of Chemical Physics and Physical Chemistry*; Moore, J. H., Spencer, N. D., Eds.; Taylor and Francis: 2001; p 2717.

(98) Ohmine, I.; Tanaka, H. *J. Chem. Phys.* **1990**, *93*, 8138–8147.

(99) Nitzan, A.; Jortner, J. *Mol. Phys.* **1973**, *25*, 713–734.

(100) Chen, X. G.; Schweitzerstenner, R.; Asher, S. A.; Mirkin, N. G.; Krimm, S. *J. Phys. Chem.* **1995**, *99*, 3074–3083.

(101) Stock, G. *Phys. Rev. Lett.* **2009**, *102*, 118301.

(102) Rey-Lafon, M.; Forel, M. T.; Garrigou-Lagrange, C. *Spectrochim. Acta* **1973**, *29A*, 471–486.